energies

MDPI

Article

Optimizing S Chemical Looping Combustion with Cu-Fe Combined Oxygen Carriers: Performance and Mechanistic Insights

Lihuai Peng and Min Zheng *

School of Metallurgy and Energy Engineering, Kunming University of Science and Technology, Kunming 650093, China; penglihuai@stu.kust.edu.cn

* Correspondence: 20130012@kust.edu.cn

Abstract: This study focuses on the S-to-H_2SO_4 industry by investigating the chemical looping combustion (CLC) process utilizing Fe-based and Cu-based oxygen carriers (OCs), which are widely applied in CLC technology. The primary objective is to conduct combined CLC reactions of these two metal carriers in a three-zone temperature tube furnace, aiming to achieve a higher SO_2 yield than what is attainable by reacting a single metal carrier with S. The investigation reveals promising industrial applications, offering potential benefits in terms of reducing equipment costs, enhancing energy efficiency, and lowering the emissions of the H_2SO_4 production industry. Through a series of experiments, the study examines the effects of reaction temperature and material molar ratios on SO_2 generation. The solid reaction products were characterized using X-ray diffraction (XRD), scanning electron microscopy with energy-dispersive spectroscopy (SEM-EDS), and X-ray photoelectron spectroscopy (XPS). The experimental results indicate that the combined Cu-based and Fe-based OCs exhibit a higher SO_2 yield during the reduction stage compared to using either Fe-based or Cu-based OCs independently. Under optimal conditions, with a carrier gas flow rate of 300 mL/min, an Fe_2O_3/S molar ratio of 6:1 in the second temperature zone, and a reaction temperature of 900 °C, the total SO_2 yield in the third temperature zone reached approximately 85%. This was achieved at a reaction temperature of 850 °C, with an Fe_2O_3/S molar ratio of 6:1 in the first half of the zone and a CuO/S molar ratio of 12:1 in the second half of the zone. SEM-EDS analysis further revealed that the combined OCs showed no significant signs of agglomeration or sintering after 10 cycles of the reaction. However, Cu-based carrier particles increased in size by 50%, while Fe-based carrier particles remained relatively stable. Additionally, the low mass-to-atom ratio of S on the surface of OCs after the cyclic reaction suggests that the reduced-state OCs can be fully oxidized and regenerated following the release of SO_2 during oxidation.

Keywords: chemical looping combustion; Cu-based oxygen carrier; Fe-based oxygen carrier; S; SO_2

Citation: Peng, L.; Zheng, M. Optimizing S Chemical Looping Combustion with Cu-Fe Combined Oxygen Carriers: Performance and Mechanistic Insights. *Energies* **2024**, *17*, 5018. https://doi.org/10.3390/en17205018

Academic Editors: Iqbal M. Mujtaba and Fabio Montagnaro

Received: 26 August 2024
Revised: 26 September 2024
Accepted: 2 October 2024
Published: 10 October 2024

1. Introduction

Chemical looping combustion (CLC) represents an innovative combustion technique and was initially identified and proposed by Richter and Knoche [1]. This method enhances the oxidative capacity of oxygen carriers (OCs) through direct reactions with lattice O present in OCs [2–4], thereby restoring their oxidizing power. Unlike conventional combustion, which involves the direct mixing of fuel with air, CLC decomposes the combustion process into two primary reactions: oxidation and reduction. In this process, metal oxides serve as OCs, and CLC system operates within two interconnected reactors: a fuel reactor (FR) and an air reactor (AR) [5,6]. CLC effectively prevents direct contact between the fuel and air, resulting in flame-free combustion, which facilitates the efficient utilization of the chemical energy contained in the fuel. This approach not only enables low-energy consumption CO_2 separation but also mitigates the formation of NO_x associated with fuel combustion [7,8].

Fossil fuels, which can be categorized as solid (e.g., coal, petroleum coke) or gaseous (e.g., natural gas), typically contain S. Natural gas is primarily composed of CH_4, but

also contains a proportion of H_2S. In coal, S exists in various forms, including organic S, inorganic S, and small quantities of elemental S. During combustion, a significant portion of S present in these fuels is oxidized to form pollutants such as SO_2, which is subsequently released into the atmosphere, contributing to environmental pollution [9]. For CLC, S in fuels can interact with OCs, resulting in several detrimental effects. Specifically, S reacts with OCs to produce metal sulfides and sulfates, which can lead to the deactivation and poisoning of OCs. This deactivation significantly diminishes their reactivity and may induce agglomeration and sintering. Following the cyclic reaction, the structural integrity of OCs becomes compromised, leading to a reduction in porosity and surface area [10]. This results in a failure to meet the performance requirements of the CLC process for high-efficiency OCs. Consequently, recent years have seen extensive research conducted by scholars, both domestically and internationally, on the effect of S in fuels on the reactivity of OCs in CLC.

Diego et al. [11] synthesized Fe-based and Cu-based OCs, utilizing Al_2O_3 as an inert support through an initial impregnation method. These OCs were subsequently exposed to a gas mixture containing 15 vol.% H_2S. The results indicated that the affinity of CuO for H_2S was superior to that of Fe_2O_3, resulting in a more stable reaction process characterized by minimal agglomeration. However, during the reduction phase, H_2S may have reacted with CuO, Cu monomers, and Cu_2O, leading to the formation of Cu_2S [12]. This reaction can result in the release of minor amounts of SO_2 into the reactor environment. Conversely, the interaction between Fe_2O_3 and H_2S does not yield FeS or 4, resulting in negligible SO_2 emissions, particularly when Fe/S ratio exceeds 1.5:1. Fe-based OCs exhibit high reactivity towards S-containing fuels and demonstrate significant resistance to S. Therefore, both Fe-based and Cu-based OCs possess different advantages regarding the combustion of high-S fuels.

In a study focused on the characterization of S migration during lignite CLC, Adánez et al. [13] selected a Cu-based OC for detailed examination. The results indicated that up to 87.9% of the S present in the fuel was converted into SO_2 and subsequently released within the FR. However, due to the incomplete gasification process of the fuel, involving Cu within the reactor, certain unconverted S species were transported to the AR, resulting in the generation of minor amounts of SO_2 in that environment. To gain a deeper understanding of the effect of various OCs on S migration, Mendiara et al. [14] employed natural ilmenite as an OC to further investigate the emission characteristics of S-containing pollutants in the gas phase during lignite CLC. Their research revealed that SO_2 and H_2S were the predominant S-containing gaseous components in the FR, and that an increase in the reaction temperature of the FR could significantly enhance the conversion of H_2S into SO_2.

García et al. [15] explored the application of CLC technology within H_2SO_4 industry, conducting CLC experiments utilizing S in a 500 wt/h thermal power CLC system. As one of the most significant industrial chemicals globally, the production of H_2SO_4 serves as a critical indicator of a country's industrial capacity. H_2SO_4 is extensively employed in the production of raw materials for phosphate fertilizers, a diverse array of chemicals, metal processing, as an electrolyte in lead–acid batteries, and for the removal of impurities in the petroleum industry. Presently, the primary raw materials utilized in the production of H_2SO_4 include S, FeS_2, and non-ferrous sulfide ores.

In the conventional production of H_2SO_4, S is initially combusted with air at elevated temperatures in a S furnace, typically at approximately 1100 °C, to generate SO_2. Subsequently, the flue gases containing SO_2 are cooled in a waste heat boiler to approximately 420 °C before being introduced into a converter, where SO_3 is produced through the catalytic oxidation of SO_2. To meet the demands of these two reactions, S furnace must be supplied with an excess of air, which results in an increased N_2 content and consequently limits the concentration of SO_2 to approximately 12 vol.% [16].

Tian et al. [17] synthesized OCs featuring CuO@TiO_2-Al_2O_3 hierarchical structures through self-assembly combustion synthesis. The combustion efficiency of OC consistently exceeded 97% after 20 reaction cycles at 900 °C, utilizing anthracite as the fuel source.

Notably, no $CuAl_2O_4$ was detected in the recycled products, and significant sintering was absent, which suggests that OCs exhibit remarkable reactivity, durability, and resistance to sintering.

García et al. [15] suggested that the implementation of CLC technology within H_2SO_4 industry is both feasible and economically advantageous. The concentration of SO_2 at the outlet of FR approaches 100 vol.%, and the SO_2 concentration introduced into the converter after mixing can be elevated to 18 vol.%, thereby significantly decreasing the overall costs associated with the acid production facility. Furthermore, the operating temperature of AR, approximately 900 °C, is considerably lower than that of a conventional S combustion furnace, which operates at approximately 1100 °C. This reduction in temperature effectively mitigates the formation of thermal NO_x. Additionally, the heat generated from the oxidation reaction can be harnessed for power generation. Therefore, the investigation of a S CLC process not only holds promise for industrial application but also bears substantial implications for cost reduction, energy conservation, and emission mitigation within the acid production sector.

In this study, the sol–gel combustion synthesis method was employed to prepare reactive Cu-based OCs and the sol–gel method was utilized to produce environmentally friendly Fe-based OCs for S CLC. The Fe_2O_3/S molar ratio was fixed at 6:1 in the second temperature zone, while the CuO/S molar ratio was set at 12:1 in the first half of the third temperature zone. The generation pattern of SO_2 from the combined Cu-based and Fe-based carriers during the reduction and oxidation stages was examined by varying the reaction temperature in the third temperature zone, with the molar ratio of Fe-based carriers adjusted in the latter half of this zone to identify the optimal conditions for an enhanced SO_2 yield. Finally, cyclic experiments were conducted on the combined Cu-based and Fe-based OCs, and the solid products were analyzed using scanning electron microscopy with energy-dispersive spectroscopy (SEM-EDS) and X-ray photoelectron spectroscopy (XPS) to assess the stability of the S CLC reactions of OCs.

2. Experiment

Pure Fe_2O_3 is insufficient to meet the demands of multiple cycles. Therefore, the incorporation of inert carriers is necessary to enhance its mechanical properties and improve wear resistance. Commonly utilized inert carriers include $MgAl_2O_3$, Al_2O_3, TiO_2, SiO_2, and ZrO_2. In the case of Fe_2O_3/TiO_2 OCs [18], the formation of Fe_2TiO_5 from the interaction between Fe_2O_3 and TiO_2 during loading results in significant sintering phenomena due to the low melting point of Fe_2TiO_5 [19]. Similarly, for Fe_2O_3/SiO_2 OCs, severe sintering occurs as a result of the generation of $FeSiO_3$ during the loading process. The $FeSiO_3$ is inert and substantially diminishes the reactivity of OCs. Consequently, it can be concluded that Fe_2O_3/SiO_2 is not an appropriate choice as an inert carrier for Fe-based OCs [20]. In contrast, $MgAl_2O_3$, Al_2O_3, and ZrO_2 do not produce spinel phases and exhibit favorable performances as inert carriers. Among these, Fe_2O_3/Al_2O_3 OC demonstrates high reactivity and resistance to sintering. Although it is less resistant to carbon accumulation, the fuel utilized in this experiment does not contain carbon, making Fe_2O_3/Al_2O_3 a viable option for S CLC. H_2 temperature-programmed reduction (H_2-TPR) experiments were conducted on Fe_2O_3/Al_2O_3 OCs prepared with varying loading ratios of 8:2, 7:3, 6:4, 5:5, 4:6, 3:7, and 2:8. A sample mass of 30 mg was introduced into a U-tube using a sol–gel method combined with self-propagating combustion synthesis. The samples were heated from room temperature to 200 °C at a rate of 10 °C/min and pretreated for 120 min in a He gas stream. Subsequently, the samples were cooled to 40 °C, and the He gas stream was replaced with a 10% H_2/He gas mixture. These conditions were maintained for 60 min to ensure gas stream stability. Finally, the samples were heated to 900 °C. H_2-TPR data for the OCs are illustrated in Figure 1. The data reveal that the Fe_2O_3/Al_2O_3 OC exhibits only two peaks, with the first peak corresponding to one reaction and the second peak corresponding to another. When the mass ratio of Fe_2O_3/Al_2O_3 approaches 5:5, the temperature of the peaks gradually increases, indicating a decline in low-temperature reducibility. Conversely,

when the mass content of Fe_2O_3 is either greater or less than 50%, the peak temperature of H_2-TPR gradually decreases, regardless of whether the percentage of active components or inert components increases. However, as the proportions of active and inert components converge, the H_2 consumption of OC gradually increases, suggesting an enhancement in reduction reaction activity. OC exhibits the highest reduction activity when the mass ratio of Fe_2O_3/Al_2O_3 is 5:5.

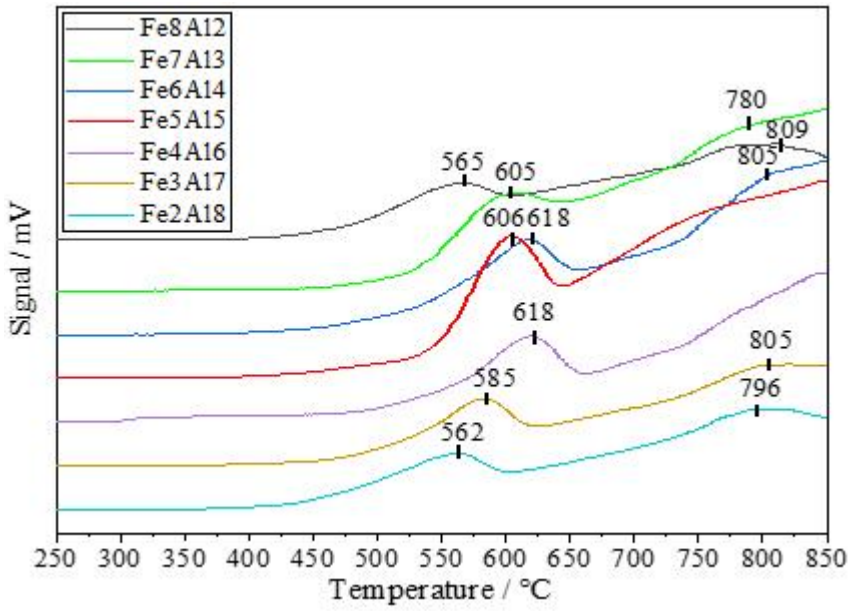

Figure 1. H_2-TPR data of Fe_2O_3/Al_2O_3 OCs.

In summary, $CuO@TiO_2$-Al_2O_3 and Fe_2O_3/Al_2O_3 OCs were synthesized using a sol–gel method in conjunction with self-propagating combustion synthesis. The preparation of Cu-based OCs involved the following steps: Cu-based OCs were prepared by weighing 3.5 g of μm-Al_2O_3 and 1 g of nm-TiO_2. These materials were subjected to ultrasonication and stirring, followed by the addition of specific proportions of poly(vinyl alcohol) and urea for dissolution. Subsequently, 47.1 g of $Cu(NO_3)_2{\cdot}3H_2O$ was incorporated to obtain a wet gel, which was stirred. The dry gel of the precursor was then obtained through combustion synthesis. The preparation of Fe-based OCs involved the following steps: For Fe-based OCs, specific proportions of $Al(OC_3H_7)_3$ and dilute nitric acid were weighed to produce a hydrolyzed γ-AlOOH sol of boehmite. A wet gel was then formed by adding 28.7 g of $Fe(NO_3)_3{\cdot}9H_2O$ while stirring. The composite Fe_2O_3/Al_2O_3 OC, with a mass ratio of 5:5, was subsequently obtained through phased drying and calcination. The cooled samples of both OCs were ground and sieved to achieve a particle size of 400 μm. They were then encapsulated in sample bags and stored under cool and dry conditions. The fuel utilized in the experiment was analytically pure industrial S, sourced from Hengxing Chemical Reagent Co., Ltd., Tianjin, China.

Figure 2 shows the entire experimental system diagram: 1. gas mass flow controller; 2. isolatable air feed device; 3. open-box three-temperature-zone tube furnace; 4. serpentine condenser tube; 5. flue gas analyzer; 6. tail gas absorption device; ①. the first temperature zone; ②. the second temperature zone; ③. the third temperature zone.

The experiments were conducted using a 3 (model TL-1200-1200-1200, Boyuntang Instrument Technology Co., Ltd., Nanjing, China). A gas cylinder was connected to the furnace through 2, and the gas flow rate was regulated by a 1. N_2 served as the carrier gas for S during the reduction reaction phase of OC, while air was utilized as the oxidizing agent during the oxidation reaction phase. The three-temperature-zone tube furnace was specifically employed for this experimental FR. The quartz tube measured 1.4 m in length, with an outer diameter of 25 mm and an inner diameter of 20 mm. A total of 64 mg

(0.002 mol) of industrial S was placed in a ceramic boat located in the first temperature zone of the furnace, while the organic compounds were positioned in the second and third temperature zones.

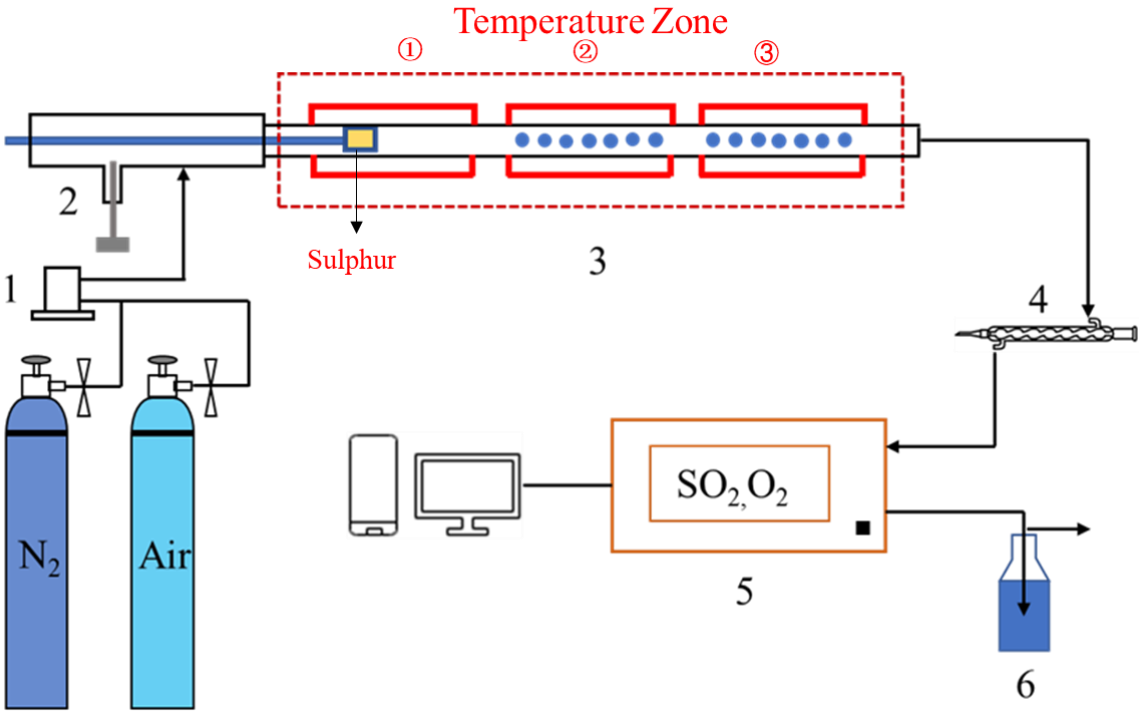

Figure 2. Experimental system diagram.

The circular CLC experiment was conducted in the following manner:

(1) ① was established at 800 °C, ② was established at 900 °C, and ③ was established at 850 °C, with a temperature increase rate of 10 °C/min. The temperature in the first zone was elevated from room temperature to 800 °C, while the second and third zones were adjusted to their respective target reaction temperatures. Subsequently, the flow of N_2 was halted, and 99.999% anhydrous high-purity air was introduced for oxidation. The air oxidation process was conducted at temperatures of 900 °C and 800 °C, with Fe-based material positioned in the second temperature zone, Cu-based organic compound located in the first half of the third temperature zone, and Fe-based organic compound situated in the second half of the third temperature zone.

(2) To conduct S CLC experiments, the reactor's atmosphere was initially purged with N_2. Subsequently, N_2 supply was ceased to prevent the premature expulsion of gasified S prior to designated reaction temperature being reached. S was heated in a N_2 atmosphere, and once S in the initial temperature zone reached its vaporization point, N_2 was introduced to transport the vapor to the second and third temperature zones for reaction with OC. Following the reduction reaction between OC and S, the concentration of SO_2 gas was analyzed using an online 5, and the SO_2 yield was subsequently calculated based on the concentration curve.

(3) After the concentration of SO_2 in the tail gas is reduced to 0%, the incoming N_2 is substituted with air to facilitate the oxidation of OC and to complete a CLC cycle. The concentrations of O_2 and SO_2 in the gas product are measured using an online 5. This analyzer has a SO_2 concentration range of 0~10% and an accuracy of 0.01%.

(4) Finally, cooling of high temperature SO_2 gas through 4, 6 is employed to absorb SO_2 from the exhaust gases, thereby mitigating the potential environmental impact when the gases are released into the atmosphere.

The calculation of the SO_2 yield from a S CLC reaction, utilizing a Cu-Fe combined OC, is presented in Equation (1):

$$\eta_{SO_2} = \frac{\int_0^t \frac{(C_{SO_2} \times V)}{60} dt}{n_s \times V_M} \quad (1)$$

where η_{SO_2} represents the yield of SO_2 (%); C_{SO_2} represents the concentration of SO_2 (vol.%); V represents the inlet gas flow rate (L/min); n_s represents the molar amount of S (mol); and V_M represents the molar volume of the gas under standard conditions (22.4 L/mol).

The synthesized catalysts were characterized through various analytical techniques, including SEM-EDS. Imaging was performed using the Nano nova SEM 450 field emission SEM manufactured by FEI Corporation, Hillsborough, CA, USA. H_2-TPR analysis was conducted utilizing a ChembetPulsarTPR/TPD chemical adsorption instrument from Quantachrome Instrument Company, Boynton Beach, FL, USA. Additionally, XPS was performed, utilizing the Thermo Scientific Apreo 2 X-ray photoelectron spectrometer from Thermo Fisher Scientific, Waltham, MA, USA, to ascertain the oxidation states of the surface elements present in the samples. X-ray diffraction (XRD) analysis was carried out using a Miniflex 600 diffractometer from Rigaku Corporation, Tokyo, Japan. These analytical methods were employed for morphological analysis, compositional analysis, the identification of electronic states, and the characterization of the catalyst structure, respectively.

The operating conditions of the entire experiment are shown in Table 1 below.

Table 1. Experimental working conditions.

Experimental Group	Installations	Sulfur/mol	The Ratio of Reactants to S	First/Second/Third Zone Reaction Temperature (°C)	Reaction Atmosphere
Experiments on Fe_2O_3 addition in the third temperature zone	Feeding device + Tube furnace with three temperature zones + Flue gas analyzer	0.002	Fe_2O_3/S = 6:1 CuO/S = 12:1 Fe_2O_3/S = 2:1, 4:1, 6:1, 8:1	800/850/900	N_2/Air (300 mL/min)
Reaction temperature experiment in the third temperature region of combined OCs	Feeding device + Tube furnace with three temperature zones + Flue gas analyzer	0.002	Fe_2O_3/S = 6:1 CuO/S = 12:1 Fe_2O_3/S = 6:1	800/900/(800, 850, 900)	N_2/Air (300 mL/min)
Combined OC cyclic experiment	Feeding device + Tube furnace with three temperature zones + Flue gas analyzer	0.002	Fe_2O_3/S = 6:1 CuO/S = 12:1 Fe_2O_3/S = 6:1	800/900/850	N_2/Air (300 mL/min)

3. Results and Discussion

3.1. Thermodynamic Calculation

The potential reactions of Cu-based OCs with S are illustrated below. The reduction of CuO by S predominantly yields Cu_2O (Equation (2)), alongside a concurrent reaction that generates Cu monomers (Equation (6)). At elevated temperatures, CuO undergoes an O_2 uncoupling reaction (Equation (3)), which facilitates the reaction of S with molecular O_2 (Equation (4)). When the reduction product is subjected to extensive reduction, it results in the formation of Cu_2S (Equations (5) and (7)). Furthermore, there exists a possibility that CuO and the extensively reduced product, Cu_2S, may continue to react, yielding Cu_2O and Cu monomers (Equations (8) and (9)). Additionally, CuO and Al_2O_3 may interact during the preparation of OCs, leading to the formation of $CuAl_2O_4$, which may subsequently react with S to produce $CuAlO_2$, Cu, and CuS. The variation in Gibbs free energy for each reaction at different temperatures is depicted in Figure 3a. From 450 °C to 1400 °C, with

the exception of reaction (Equation (3)), all other reactions exhibit Gibbs free energies of less than 0, indicating that these reactions are thermodynamically favorable.

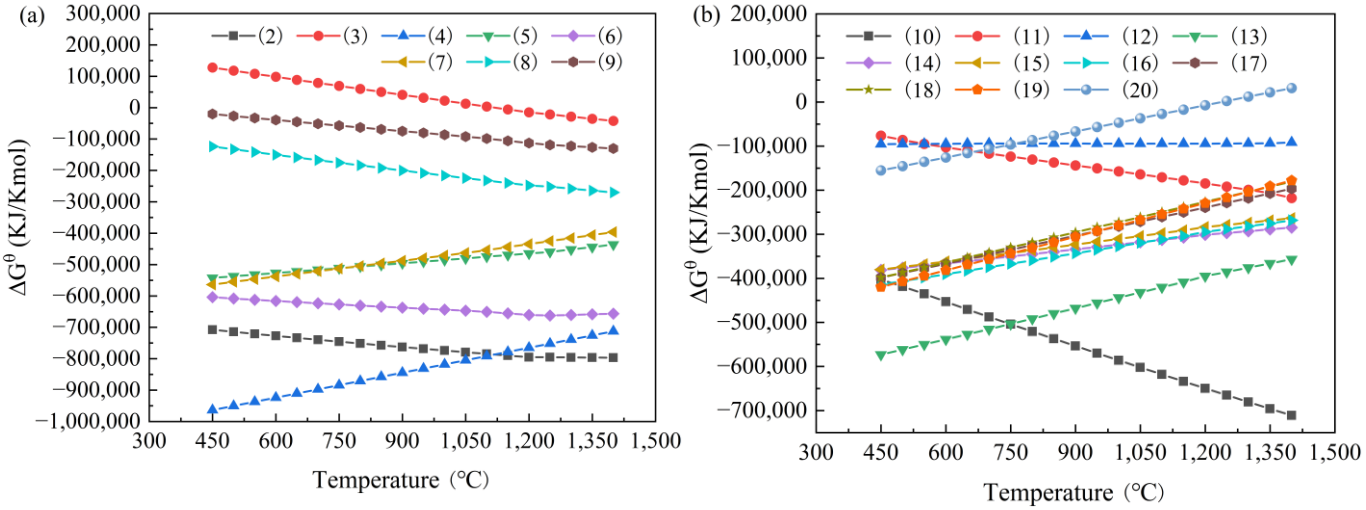

Figure 3. Gibbs free energy of possible reactions: (**a**) S with CuO; (**b**) S with Fe_2O_3.

Reactions that can occur in fuel reactors with Cu-based OCs:

$$2S_{(g)} + 8CuO = 4Cu_2O + 2SO_{2(g)} \quad (2)$$

$$4CuO = 2Cu_2O + O_{2(g)} \quad (3)$$

$$2S_{(g)} + 2O_{2(g)} = 2SO_{2(g)} \quad (4)$$

$$2S_{(g)} + 4/3Cu_2O = 4/3Cu_2S + 2/3SO_{2(g)} \quad (5)$$

$$2S_{(g)} + 4CuO = 4Cu + 2SO_{2(g)} \quad (6)$$

$$2S_{(g)} + 4Cu = 2Cu_2S \quad (7)$$

$$Cu_2S + 6CuO = 4Cu_2O + SO_{2(g)} \quad (8)$$

$$Cu_2S + 2CuO = 4Cu + SO_{2(g)} \quad (9)$$

The combustion of Fe-based OCs in the presence of S within FRs constitutes a complex reaction process. During the reduction of Fe-based OCs by S, S primarily reacts with Fe_2O_3 to yield Fe_3O_4 (Equation (10)). However, with the ongoing interaction between the reduction products and S, Fe_3O_4 may be progressively reduced to form the low-valent metal oxide FeO (Equation (11)) as well as the elemental metal Fe (Equation (12)). Additionally, the respective reduction products of Fe-based OCs may react with S to produce metal sulfides, including FeS (Equations (13), (15) and (16)) and FeS_2 (Equations (18)–(20)). At high temperatures, Fe_2O_3 and Al_2O_3 may also react to generate $FeAl_2O_4$, which can subsequently react with S to produce FeS. In summary, in contrast to Cu-based OCs, Fe-based OCs can undergo gradual reduction during their reaction with S, resulting in the formation of various reduction products such as Fe_3O_4, FeO, and Fe. This process, to a certain extent, mitigates the formation of metal sulfides. The results from subsequent experiments have corroborated this observation.

Reactions that can occur in fuel reactors with Fe-based OCs:

$$2S_{(g)} + 12Fe_2O_3 = 8Fe_3O_4 + 2SO_{2(g)} \quad (10)$$

$$2S_{(g)} + 4Fe_3O_4 = 12FeO + 2SO_{2(g)} \quad (11)$$

$$2S_{(g)} + 4FeO = 4Fe + 2SO_{2(g)} \quad (12)$$

$$2S_{(g)} + 2Fe = 2FeS \quad (13)$$

$$2S_{(g)} + 4/7Fe_2O_3 = 8/7FeS + 6/7SO_{2(g)} \quad (14)$$

$$2S_{(g)} + 2/5Fe_3O_4 = 6/5FeS + 4/5SO_{2(g)} \quad (15)$$

$$2S_{(g)} + 4/3FeO = 4/3FeS + 2/3SO_{2(g)} \quad (16)$$

$$2S_{(g)} + 4/11Fe_2O_3 = 8/11FeS_2 + 6/11SO_{2(g)} \quad (17)$$

$$2S_{(g)} + 2/8Fe_3O_4 = 6/8FeS_2 + 2/4SO_{2(g)} \quad (18)$$

$$2S_{(g)} + 4/5FeO = 4/5FeS_2 + 2/5SO_{2(g)} \quad (19)$$

$$2S_{(g)} + Fe = FeS_2 \quad (20)$$

The variation in Gibbs free energy for each reaction involved in the S reduction of Fe_2O_3 at various reaction temperatures is depicted in Figure 3b. Between 450 °C and 1400 °C, Gibbs free energies for reactions (Equation (10)) through (Equation (19)) are all negative, suggesting that these reactions are thermodynamically favorable. However, at temperatures exceeding 1200 °C, the Gibbs free energy for the reaction (Equation (20)) becomes positive, indicating that the occurrence of this reaction becomes increasingly unfavorable at elevated temperatures (>1200 °C).

Fe oxides, specifically Fe_3O_4 and Fe_2O_3, and elemental Fe react with S to produce FeS and FeS_2. Similarly, Cu, Cu_2O, and CuO can react with S to yield CuS and Cu_2S, a process that remains thermodynamically favorable. When Fe_2O_3 undergoes excessive reduction to FeO and Fe, it readily reacts with S, resulting in the formation of metal sulfides such as FeS and FeS_2. The reduction of Cu_2O to Cu_2S can also lead to the generation of metal sulfides, which may cause the poisoning of OCs, thereby diminishing their reactivity and cyclic efficiency. This rapid deactivation of OCs hinders their ability to undergo multiple cycles and contributes to the production of elevated concentrations of SO_2 gas. Consequently, in industrial applications, it is imperative to avoid the excessive reduction of Fe_2O_3 and CuO, while also minimizing the formation of metal sulfides.

3.2. S CLC of Cu-Based OC

3.2.1. Effect of Reaction Temperature

The investigation focused on the generation pattern of SO_2 during the combustion process of Cu-based OCs at varying temperatures, based on a chemical equivalence ratio of CuO/S of 12:1. The patterns of SO_2 generation and O_2 release during the combustion reaction of Cu-based OCs with S at temperatures of 800 °C, 850 °C, and 900 °C are illustrated in Figure 4a, 4b, and 4c, respectively.

At 800 °C, the maximum O_2 concentration observed during OC reduction stage was 0.15 vol.%, while the minimum concentration recorded was 0.09 vol.%. At this temperature, the extent of O_2 release from CuO was minimal, and O_2 was scarcely involved in the reaction, which predominantly consisted of the interaction between CuO and S. As the reaction temperature increased, the degree of O_2 release from CuO exhibited a significant enhancement. At 850 °C, the peak O_2 concentration during OC reduction stage reached 0.48 vol.%. Throughout the reduction process, O_2 was continuously released and consumed by S, resulting in a decrease in the O_2 concentration to a minimum of 0.23 vol.% near the peak SO_2 concentration of 5.55 vol.%. During this reduction phase, CuO and O_2 released can react with S, while the reduction products, Cu_2O and metallic Cu, may also react with S to form Cu_2S. Additionally, a portion of S may exist in the form of metal sulfide, allowing the SO_2 concentration during the oxidation phase to reach 4.5 vol.%. At 900 °C, CuO exhibited a higher degree of O_2 release during the reduction stage, with O_2 concentrations reaching up to 1.3 vol.%. As the reduction reaction progressed, the O_2 concentration decreased to 0.14 vol.%. The peak SO_2 concentration during OC reduction stage was recorded at 4.44 vol.%, whereas the SO_2 concentration during the oxidation stage attained levels as high as 6.14 vol.%.

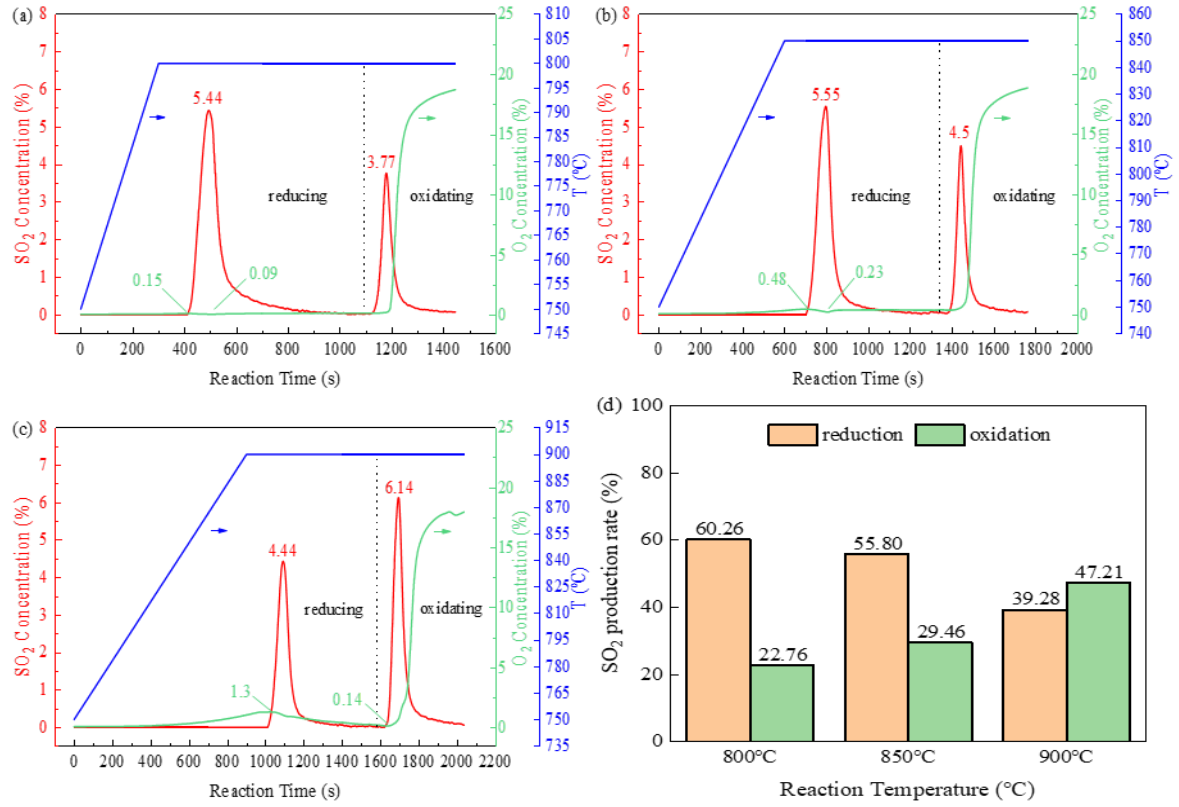

Figure 4. Effect of reaction temperature on SO_2 production: (**a**) 800 °C; (**b**) 850 °C; (**c**) 900 °C; (**d**) SO_2 yield.

The yields of SO_2 at various reaction temperatures are depicted in Figure 4d. At lower reaction temperatures, during the reduction phase of OC, SO_2 yields were recorded at 60.26%, 55.80%, and 39.28%, while the yields during the oxidation phase were 22.76%, 29.46%, and 47.21%. Notably, as the reaction temperature increases, there is a significant rise in the SO_2 yield during the oxidation phase, accompanied by an increase in the duration required for oxidation. The elevation of reaction temperature results in the release of substantial amounts of SO_2 into AR, indicating that Cu-based OCs are not suitable for S CLC reactions.

3.2.2. Effect of CuO/S Molar Ratio

For the reduction reaction involving OCs, CuO facilitates the release of O_2, which in turn oxidizes SO_2 to promote the formation of SO_3. This process leads to a reduction in the yield of SO_2. Therefore, a fixed quantity of 0.012 mol of Fe_2O_3 as an OC was shown in the second temperature zone. Additionally, the quantity of Cu-based OC introduced in the third temperature zone was varied to enhance the yield of SO_2 and to ascertain the optimal molar ratio of CuO to S.

In this series of experiments, the effect of varying CuO/S molar ratios in the combined OCs on SO_2 generation was examined, utilizing a Cu-based OC at a reaction temperature of 800 °C and a flow rate of 300 mL/min. In Figure 5, the total yields for CuO/S molar ratios, ranging from low to high, were recorded at 91.52%, 91.68%, 91.16%, 90.61%, and 91.25%, respectively. The SO_2 yield during the reduction phase of OCs exhibited a notable increase with the elevation of CuO/S molar ratio, whereas SO_2 yield during the oxidation phase demonstrated a consistent decline as the CuO/S molar ratio increased. Notably, at a CuO/S molar ratio of 12:1, the SO_2 concentration peaked at 6.25 vol.%, with the SO_2 yield in the reduction phase of the OC reaching a maximum of 78.60%.

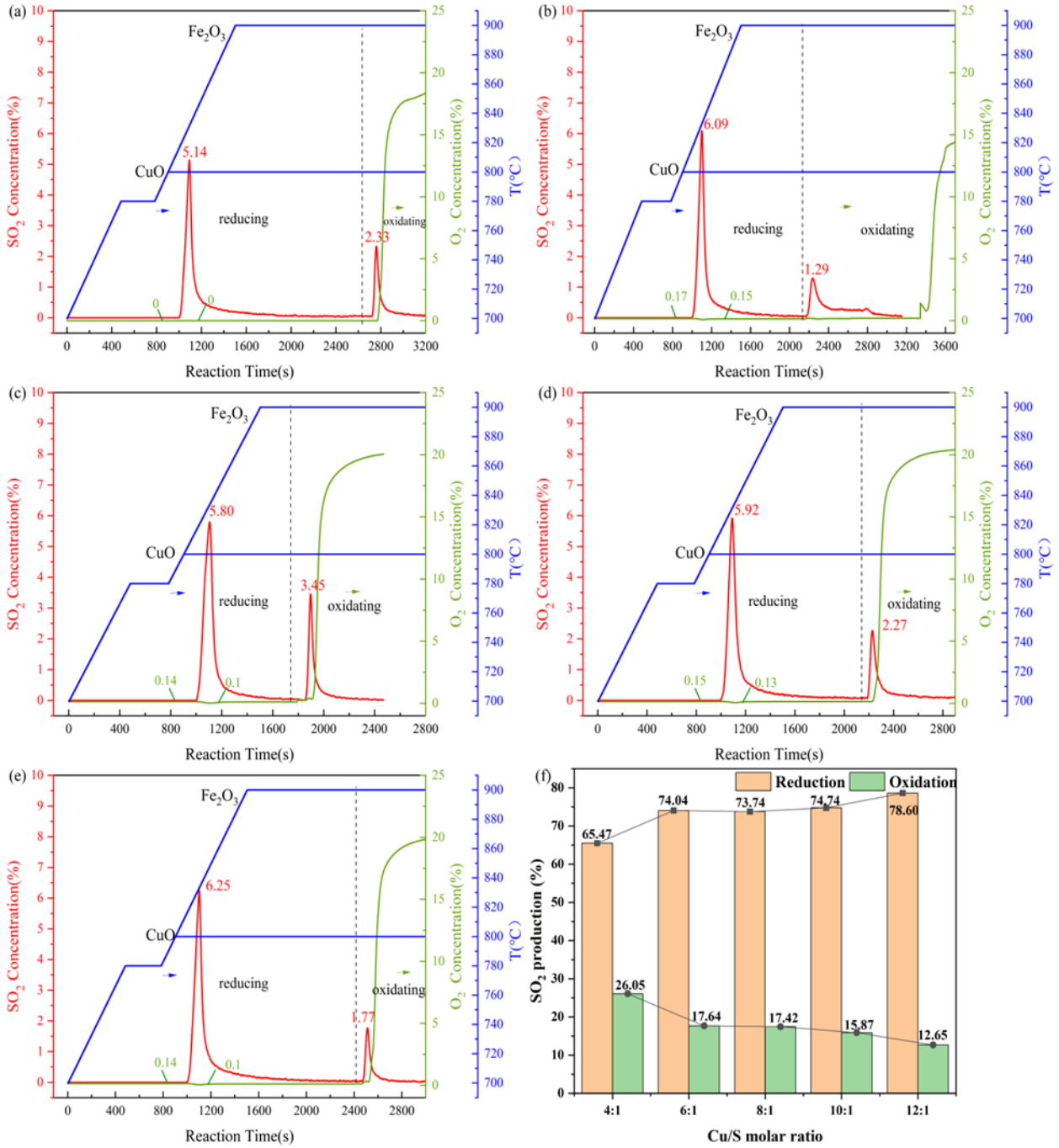

Figure 5. Effect of CuO molar ratio on SO_2 production: (**a**) 4:1; (**b**) 6:1; (**c**) 8:1; (**d**) 10:1; (**e**) 12:1; (**f**) SO_2 yield.

In summary, it is more suitable to conduct the subsequent reaction at a CuO/S molar ratio of 12:1.

3.3. S CLC of Fe-Based OCs

3.3.1. Effect of Reaction Temperature

In this section, an Fe_2O_3/Al_2O_3 composite OC with a mass loading ratio of 1:1 was prepared. SO_2 generation pattern of an Fe-based OC, which reacted with S at temperatures of 800 °C, 850 °C, 900 °C, and 950 °C, was investigated based on a chemical equivalent ratio (Fe_2O_3/S molar ratio of 6:1). The research results are presented in Figure 6.

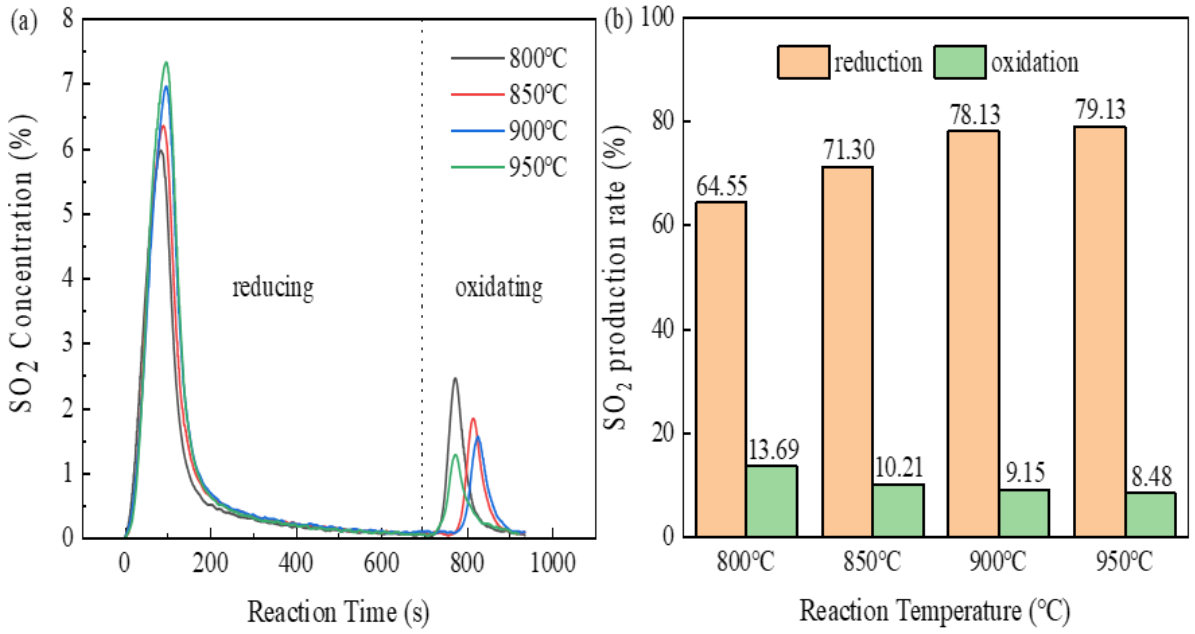

Figure 6. Effect of reaction temperature on SO_2 production: (**a**) SO_2 concentration; (**b**) SO_2 yield.

The peak concentration of SO_2 during the reduction phase of the carrier exhibited an increasing trend with rising reaction temperatures, recording values of 5.96 vol.%, 6.34 vol.%, 6.95 vol.%, and 7.32 vol.%, respectively. Conversely, the corresponding SO_2 concentrations during the oxidation phase demonstrated a decreasing trend, with values of 2.45 vol.%, 1.83 vol.%, 1.55 vol.%, and 1.27 vol.%, respectively. SO_2 yields during the reduced oxidation phase at varying reaction temperatures are illustrated in Figure 6b. SO_2 yields in the reduction phase of OC were 64.55%, 71.30%, 78.13%, and 79.13% as the reaction temperatures increased from low to high. Notably, at 800 °C, the SO_2 yield in the reduction phase was only 64.55%, whereas at 900 °C, it increased to 79.13%. This indicates that elevating the reaction temperature significantly enhances the reactivity of the carrier with S, thereby improving the fuel conversion rate. Furthermore, an increase in reaction temperature also resulted in a reduction in SO_2 release during the oxidation phase of the carrier, with SO_2 yields decreasing from 13.69% to 8.48%. At both 900 °C and 950 °C, SO_2 yields in the reduction phase of the carrier were comparable. However, the energy consumption escalated considerably with the increase in reaction temperature. Therefore, a reaction temperature of 900 °C is more suitable for attaining an optimal performance.

3.3.2. Effect of Fe_2O_3/S Molar Ratio

During the combustion reaction of Fe-based OCs with S, S primarily reacts with Fe_2O_3. However, it can also interact with reduced forms such as Fe_3O_4, FeO, and even elemental Fe. This subsection investigates the effect of varying Fe_2O_3/S molar ratios (3:1, 6:1, 9:1, and 12:1) on the generation of SO_2 during the combustion process, conducted at a reaction temperature of 900 °C. As Fe_2O_3/S molar ratio increases, the concentration of SO_2 during the reduction stage also rises, with recorded values of 6.31 vol.%, 6.95 vol.%, 7.15 vol.%, and 7.36 vol.%, respectively. Conversely, the concentration of SO_2 in the oxidation stage consistently decreases, with values of 1.89 vol.%, 1.55 vol.%, 1.34 vol.%, and 1.21 vol.%, respectively. Notably, a decrease in the Fe_2O_3 molar ratio prolongs the time required for the oxidation of OC, suggesting a higher degree of reduction of Fe_2O_3. At an Fe_2O_3/S molar ratio of 3:1, the reduction process likely results in the generation of greater quantities of Fe_3O_4, FeO, Fe, FeS, and FeS_2 compared to other Fe_2O_3/S molar ratios due to the more extensive reduction facilitated by the carrier O_2.

The yields of SO_2 during the reduction phase at various Fe_2O_3/S molar ratios are depicted in Figure 7b. As Fe_2O_3/S molar ratio increases, SO_2 yields of OCs in the reduction

phase were recorded at 73.10%, 78.13%, 76.45%, and 76.85%, respectively. Notably, the SO_2 yield in the reduction phase initially increased and subsequently decreased, reaching a maximum value of 78.13% at an Fe_2O_3/S molar ratio of 6:1. Conversely, SO_2 yield in the oxidation phase exhibited a gradual decline from 10.82% to 6.53%. Overall, an Fe_2O_3/S molar ratio of 6:1 appears to represent the most favorable experimental condition.

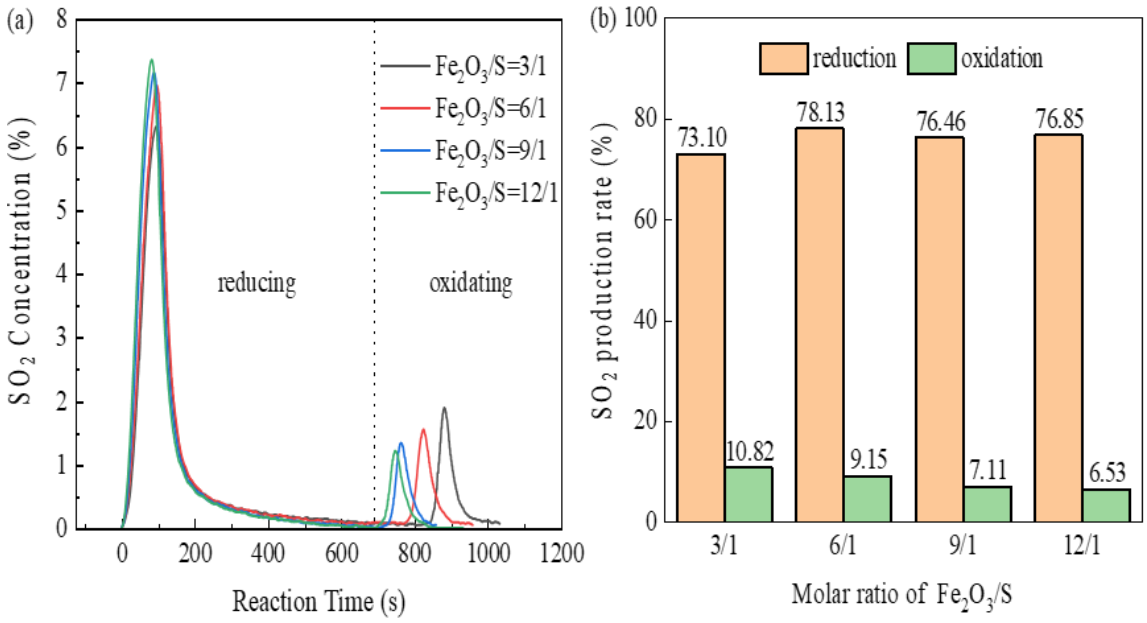

Figure 7. Effect of Fe_2O_3/S molar ratio on SO_2 production: (**a**) SO_2 concentration; (**b**) SO_2 yield.

3.4. Effect of Fe_2O_3 Addition in the Third Temperature Zone in Combined OCs

This series of experiments was conducted at a reaction temperature of 800 °C in the first temperature zone, at a reaction temperature of 900 °C in the second temperature zone, and at a reaction temperature of 850 °C in the third temperature zone. The addition of Fe_2O_3 in the first half of the third temperature zone was varied by incorporating Fe_2O_3/S with a molar ratio of 6:1 in the second temperature zone, while CuO/S with a molar ratio of 12:1 was introduced in the latter half of the third temperature zone. The flow rate during the experiments was maintained at 300 mL/min. The effect of varying molar ratios of Fe_2O_3 in the combined OC during the third temperature zone on SO_2 generation was investigated. In Figure 8, the total SO_2 yields were recorded at 84.90%, 82.91%, 86.39%, and 85.33% for Fe_2O_3/S molar ratios, ranging from low to high, respectively. SO_2 yields of the combined OCs during the reduction stage exhibited a gradual increase with the rising Fe_2O_3/S molar ratio, whereas those in the oxidation stage demonstrated a linear decrease followed by an increase as the Fe_2O_3/S molar ratio increased. These results indicate that enhancing the loading of Fe-based OCs can significantly diminish the SO_2 yield of OCs in the oxidation stage while concurrently increasing the SO_2 yield of OCs in the reduction stage. At an Fe_2O_3/S molar ratio of 6:1, the SO_2 concentration peaked at 6.17 vol.%, and the SO_2 yield in the reduction stage of OC reached a maximum of 78.62%, suggesting that this molar ratio represents an optimal condition for the reaction. Consequently, an Fe_2O_3/S molar ratio of 6:1 is more suitable for subsequent reactions.

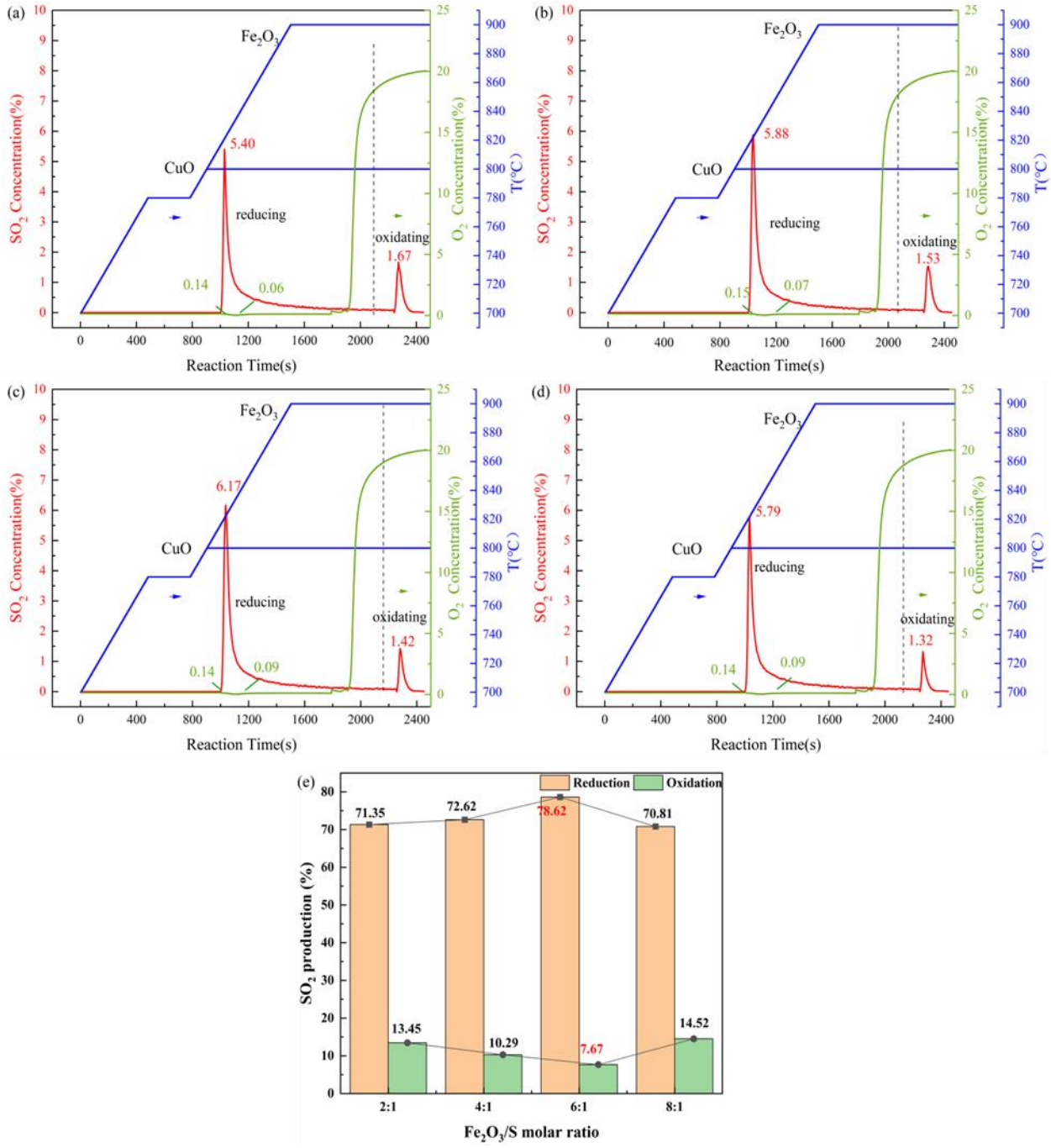

Figure 8. Effects of Fe_2O_3 addition on SO_2 generation: (**a**) 2:1; (**b**) 4:1; (**c**) 6:1; (**d**) 8:1; (**e**) SO_2 yield.

3.5. Effect of Reaction Temperature in the Third Temperature Zone in Combined OCs

The pattern of SO_2 generation at various reaction temperatures within the third temperature zone is illustrated in Figure 9. During the process in which an Cu-based OC is positioned in the front and an Fe-based OC is positioned at the back of the third temperature zone, with reaction temperatures ranging from 800 °C to 900 °C, the peak SO_2 concentrations during the reduction stage are 5.87 vol.%, 6.73 vol.%, and 6.28 vol.%, respectively. Correspondingly, SO_2 yields exhibit a similar trend, registering at 72.68%, 76.67%, and 74.07%. The redox reaction between OC and S is characterized as an endothermic process. Therefore, an increase in temperature facilitates the progression of the reaction. However, excessively high temperatures may lead to the sintering of OC samples. In this series of experiments, SO_2 concentration and yield initially increase with the temperature, reaching a

maximum before subsequently declining. This results in a pattern where both extremes are elevated while the midpoint is lower. Notably, at a reaction temperature of 850 °C within the third temperature zone, the SO_2 concentration and yield generated from the interaction between the combined OC and S peak, with a total SO_2 yield of 85.42%. In conclusion, a reaction temperature of 850 °C in the third temperature zone is identified as the most suitable condition for combustion experiments into S CLC when utilizing combined OCs.

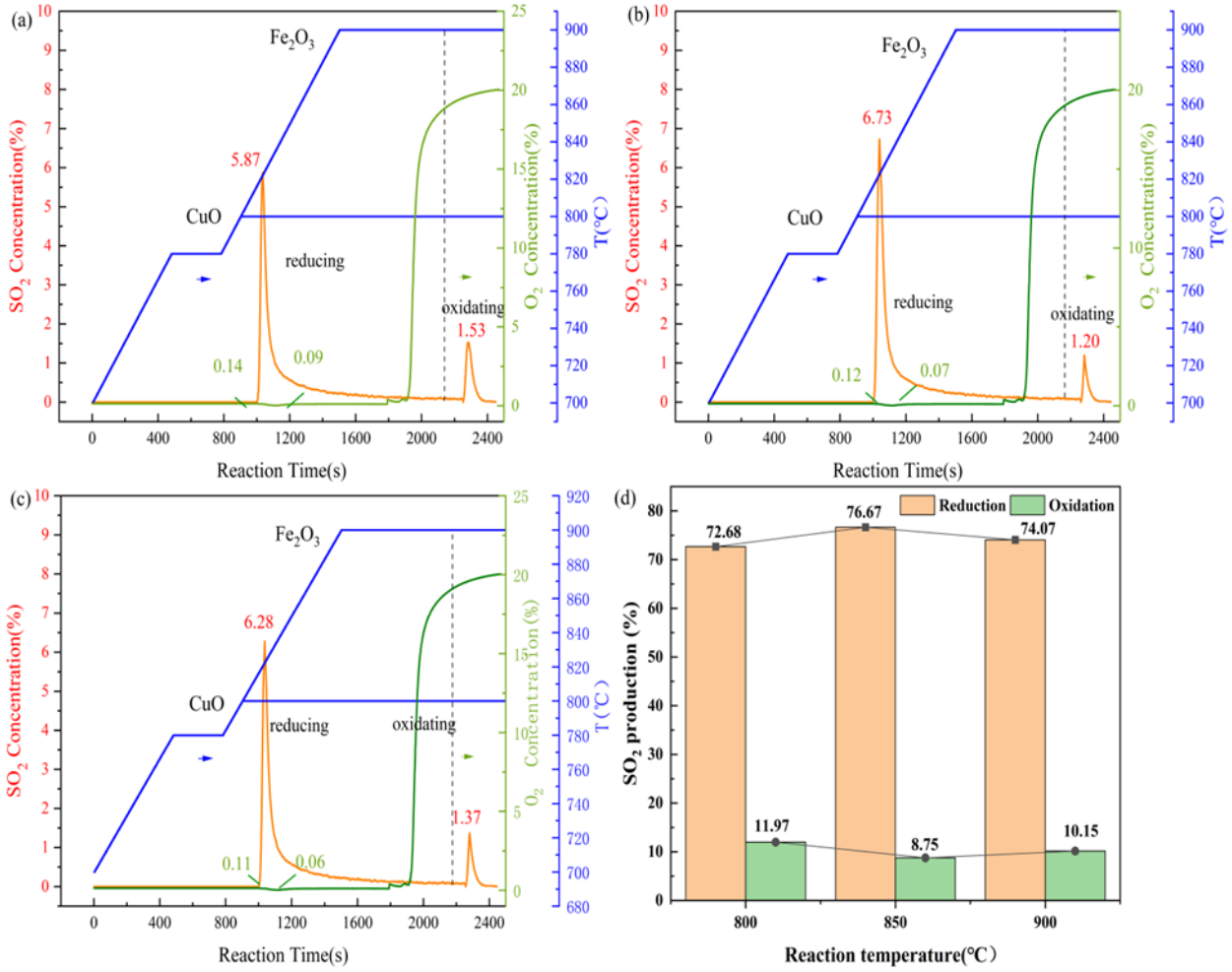

Figure 9. Effect of reaction temperature on SO_2 generation: (**a**) 800 °C; (**b**) 850 °C; (**c**) 900 °C; (**d**) SO_2 yield.

3.6. Cyclic Performance Testing of Catalysts

Under the condition that the reaction temperatures in the three zones were set at 800 °C, 850 °C, and 900 °C, respectively, the circular performance of the combined OC and S CLC was evaluated. The experimental parameters included a 6:1 Fe_2O_3/S ratio in the second temperature zone and a 12:1 CuO/S ratio in the latter half of the third temperature zone, with a gas flow rate of 300 mL/min. SO_2 generation patterns over 10 cycles during the reduction and oxidation processes are depicted in Figure 10. SO_2 concentrations recorded during the reduction phase of the 10 cycles were 5.88 vol.%, 6.73 vol.%, 7.69 vol.%, 9.16 vol.%, 9.38 vol.%, 9.41 vol.%, 9.53 vol.%, 9.63 vol.%, 9.68 vol.%, and 9.77 vol.%, respectively. In contrast, SO_2 concentrations during the oxidation phase were 1.53 vol.%, 1.51 vol.%, 1.48 vol.%, 1.39 vol.%, 1.39 vol.%, 1.35 vol.%, 1.28 vol.%, 1.23 vol.%, 1.21 vol.%, and 1.22 vol.%, respectively. Furthermore, the SO_2 yield of OC exhibited a gradual increase from 75.99% to 78.52% during the reduction stage, while it decreased from 8.20% to 7.12% during the oxidation stage. Following the initial reduction–

oxidation reaction, the performance of the OC was activated. As the number of circular reactions increased, the peak SO_2 concentration in the reduction stage demonstrated a general upward trend, accompanied by a continuous increase in SO_2 yield. Although the peak SO_2 concentration in the oxidation stage remained relatively stable, SO_2 yield consistently declined. Throughout the 10 cycles, OCs maintained high reactivity without deactivation, indicating superior circular reaction performances and enhanced stability.

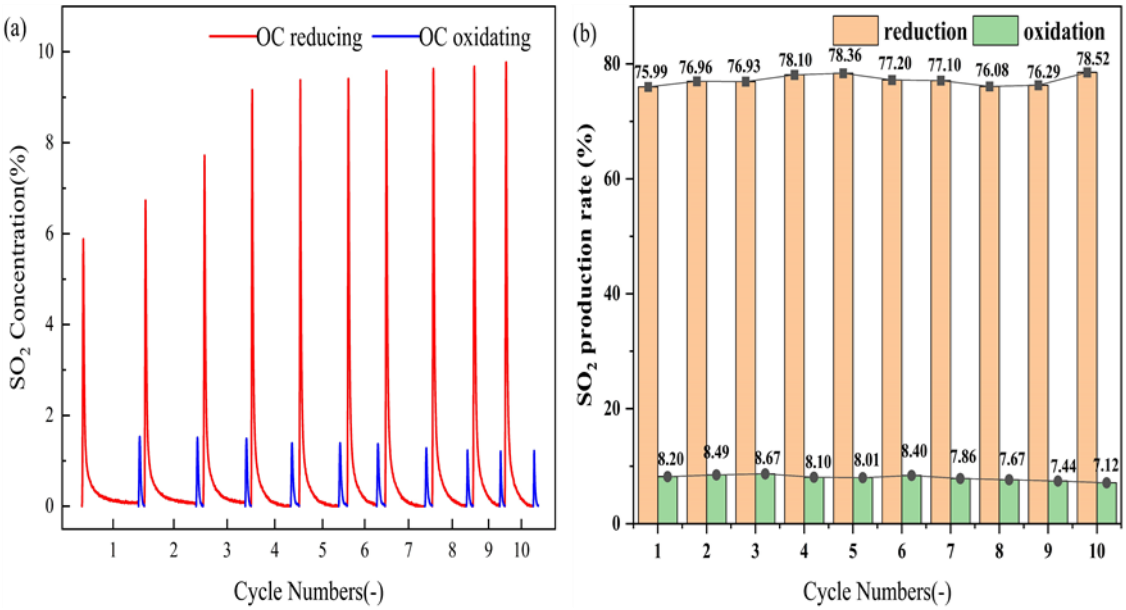

Figure 10. Circular reactions of combined Fe-based and Cu-based OCs: (**a**) SO_2 concentration curve; (**b**) SO_2 yield.

3.7. Characterization of Catalysts

3.7.1. SEM-EDS Characterization of Fresh Samples and Circulating Products

SEM-EDS characterization was conducted on fresh Fe-based and Cu-based OCs, as well as on combined OCs following ten circular reactions. The morphologies and elemental distributions of the OCs are illustrated in Figures 11 and 12, respectively.

The freshly synthesized Fe_2O_3/Al_2O_3 OC particles exhibit a uniform size, standing at approximately 100 nm, and demonstrate minimal agglomeration or sintering, resulting in a relatively loose structural configuration. EDS analysis reveals a homogeneous distribution of elements within the freshly prepared Fe_2O_3/Al_2O_3 OCs, with Fe and Al elements present in a nearly 1:1 mass ratio, indicating satisfactory loading results. Following ten cycles of S CLC reactions, the elemental distribution within OC particles remained uniform, and the overall structure continued to exhibit a loose configuration without significant agglomeration or sintering. Furthermore, the mass and atomic proportions of S in OC after the cyclic reactions were found to be exceedingly low, at only 0.06% and 0.05%, respectively. These results suggest that Fe-based OCs possess commendable S resistance, and the reduced OCs can be fully oxidized and regenerated after the release of SO_2 through oxidation.

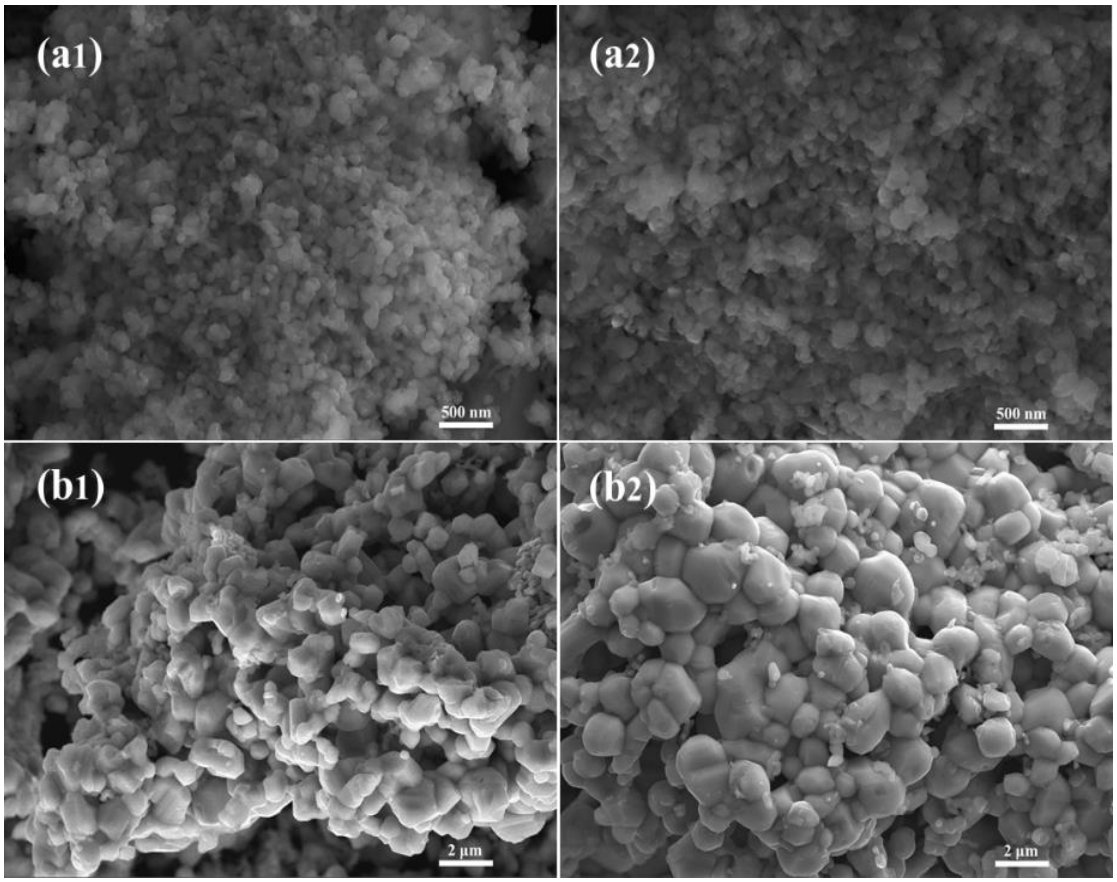

Figure 11. SEM images of Fe-based and Cu-based OCs: (**a1**) Fe-based OC before reaction; (**a2**) Fe-based OC after reaction; (**b1**) Cu-based OC before reaction; (**b2**) Cu-based OC after reaction.

$CuO@TiO_2$-Al_2O_3 fresh OCs exhibit a favorable pore structure, characterized by a generally loose and porous configuration. The particle size of OCs is relatively uniform, measuring at approximately 1 μm. Based on the calculations of the raw material ratios, the mass proportions of the constituent elements are determined to be 77.5 wt.% for Cu, 17.5 wt.% for Al, and 5 wt.% for Ti. However, EDS results reveal actual proportions of 82.42 wt.% for Cu, 3.3 wt.% for Al, and 2.96 wt.% for Ti, indicating the significant loading of CuO for the TiO_2-Al_2O_3 support template. After undergoing 10 cycles of reaction, the particle size of $CuO@TiO_2$-Al_2O_3 OCs increases to approximately 1.5 μm. Notably, there is no evident agglomeration or sintering observed, and the pore structure remains intact, preserving its loose and porous characteristics. Furthermore, the distribution of Cu and Al elements is relatively uniform, with no significant accumulation at specific locations. In comparison to the fresh samples, S content in OCs after 10 cycles of S CLC reactions does not exhibit an increase, with both the mass and atomic proportions of S remaining at 0.02%. This result suggests that Cu-based OCs possess a commendable oxidation regeneration capability within ARs.

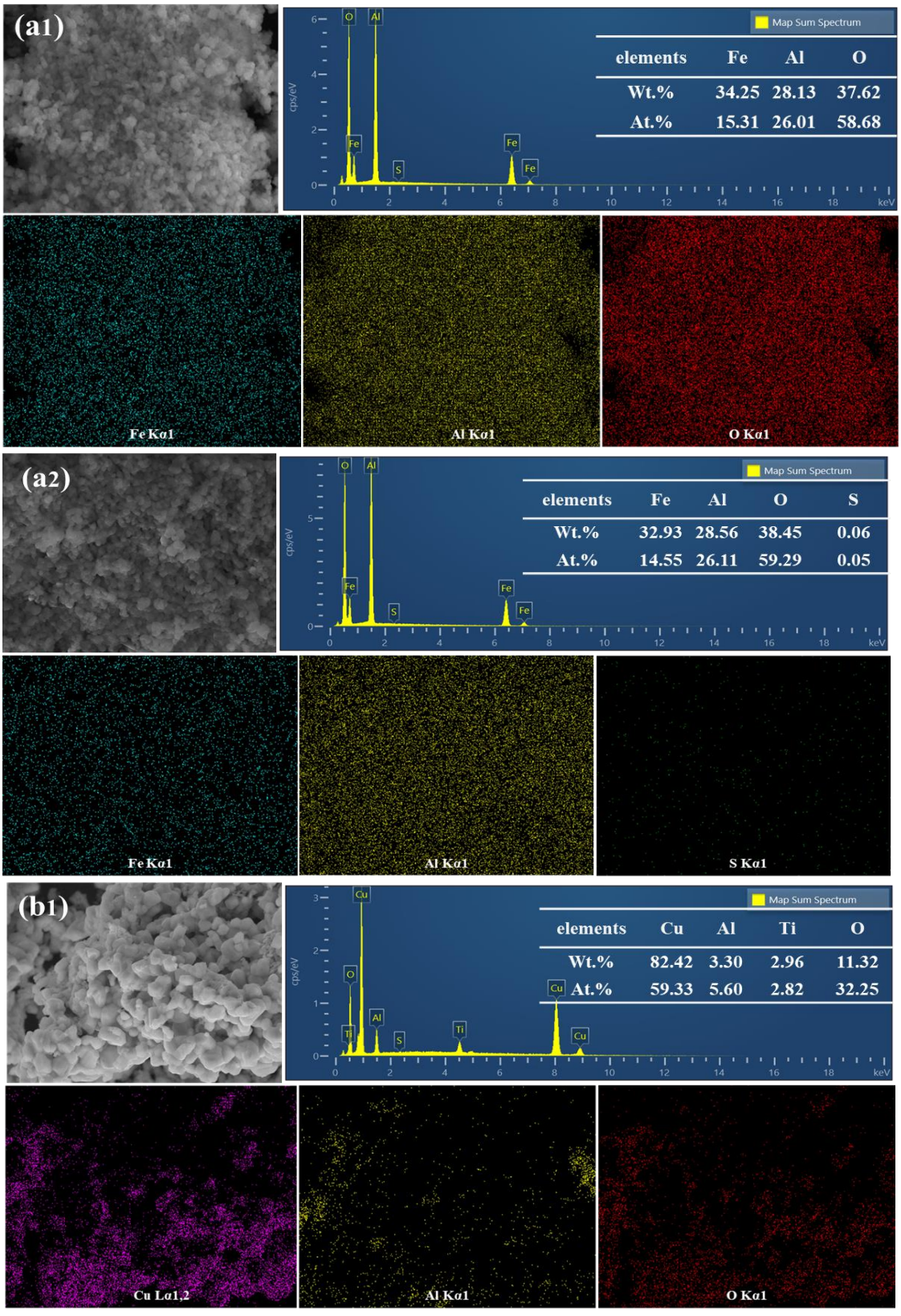

Figure 12. *Cont.*

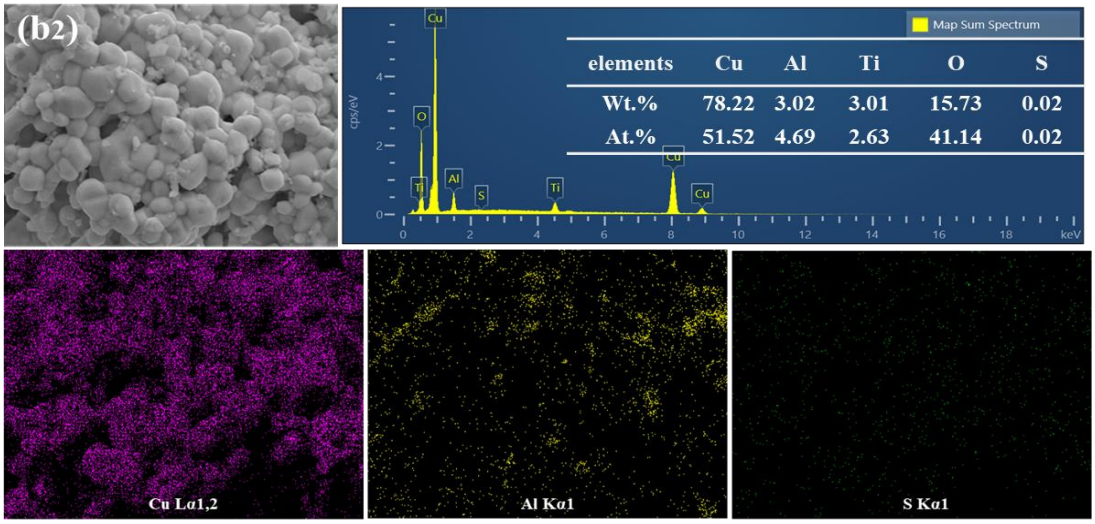

Figure 12. Elemental distribution and proportion of Cu-based and Fe-based OCs: (**a1**) Fe-based OC before reaction; (**a2**) Fe-based OC after reaction; (**b1**) Cu-based OC before reaction; (**b2**) Cu-based OC after reaction.

3.7.2. XRD and XPS Characterization of Reduction Products

Our XRD analysis of S reduction products, derived from Fe-based and Cu-based OCs, at varying reaction temperatures is presented in Figure 13. In Figure 13a, the primary products resulting from the reduction of Fe_2O_3/Al_2O_3 by S include $FeAl_2O_4$, Fe_2O_3, and Al_2O_3. This observation suggests that the reduced forms of Fe_2O_3 and Al_2O_3 can yield an Fe-Al spinel phase at elevated temperatures, characterized by the specific structure $[Fe_{0.878}Al_{0.122}][Al_{1.878}Fe_{0.122}]O_4$. Furthermore, the analysis of SO_2 generation from Fe-based OCs across different temperatures indicates that SO_2 yields in AR were 13.59%, 10.21%, 9.15%, and 8.48%, respectively, corresponding to increasing reaction temperatures. Notably, the reduction products were not detected in the presence of S monomers. Consequently, it can be inferred that a portion of the elemental S may exist in the form of metal sulfides. The detection of these metal sulfides through XRD may be hindered due to their low concentrations and suboptimal crystallization states.

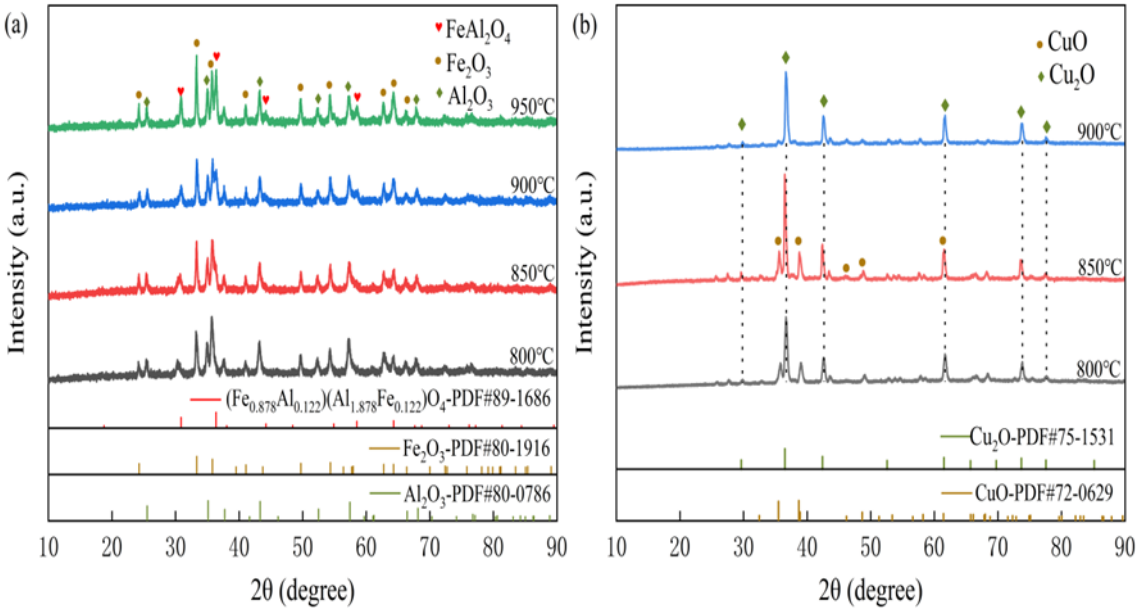

Figure 13. XRD analysis of reduction products: (**a**) Fe-based; (**b**) Cu-based.

In Figure 13b, the primary product of S reduction reactions involving Cu-based OCs at 900 °C is predominantly Cu_2O. At temperatures of 800 °C and 850 °C, the principal reduction product is also Cu_2O, along with residual CuO that has not undergone a complete reaction. XRD analyses, conducted on the reduction products obtained from experiments repeated at three temperature settings (800 °C, 850 °C, and 900 °C), did not reveal the presence of metal sulfides or Cu-Al spinel. This absence may be attributed to either a poor crystalline state or a low concentration of these compounds.

XPS fine spectra of S in the reduction products of Fe-based and Cu-based OCs are presented in Figure 13. In Figure 14a, two peaks are observed in the S 2p region. The peak at a binding energy of approximately 161.64 eV corresponds to the valence state of S as S^{2-} [21], suggesting the presence of elemental S in the form of FeS. The peak at a binding energy of approximately 168.83 eV indicates that S exists as a sulfate, likely resulting from the reaction of FeS with O_2 to form $FeSO_4$ upon exposure to air. In Figure 14b, two peaks are also observed in the S 2p region. The peak at a binding energy of approximately 162.07 eV suggests that S is present in the form of Cu_2S [22], while the peak at approximately 168.88 eV indicates the presence of S as a sulfate.

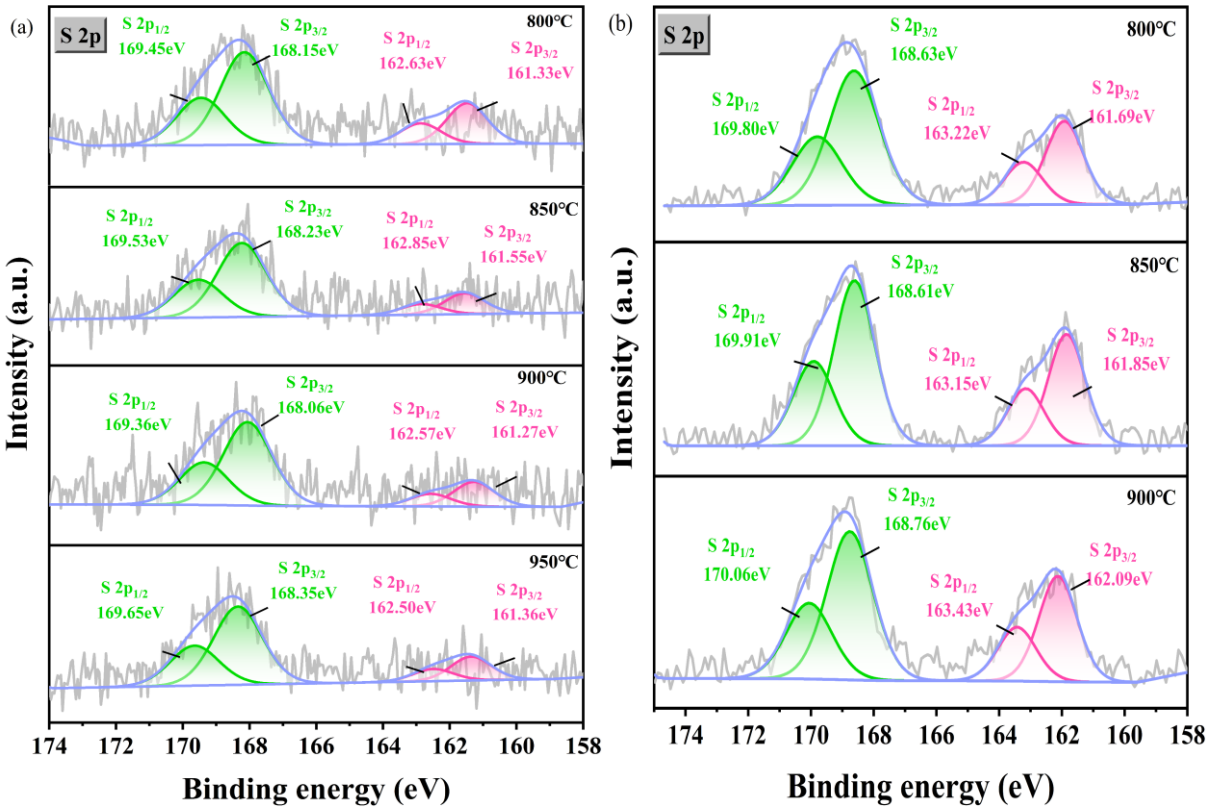

Figure 14. XPS spectra of reduction products: (**a**) Fe-based; (**b**) Cu-based.

In summary, the reduction process of OC involves an over-reduction by S, resulting in the presence of S in the form of metal sulfides, such as FeS and Cu_2S. Therefore, when the reduced state of the organic compound is oxidized by air in AR, SO_2 is released. This release is attributed to the oxidative regeneration of FeS and Cu_2S into Fe_2O_3 and CuO.

4. Conclusions

The experimental results demonstrate that the combination of Fe-based and Cu-based OCs, when fixed in the same temperature zone (third temperature zone), can achieve a higher SO_2 yield at lower reaction temperatures compared to individual metal carriers for S CLC. After 10 reaction cycles, the SO_2 yield during the reduction stage of the combined OCs exhibited an overall increasing trend, while the yield during the oxidation stage

decreased gradually. This indicates that the combined OCs possess strong cyclic reactivity and stability. SEM-EDS analysis revealed that, after 10 cycles, Cu-based and Fe-based OCs did not undergo significant agglomeration or sintering, and they retained a favorable pore structure. However, the particle size of Cu-based OC increased from approximately 1 μm to 1.5 μm, while the particle size of Fe-based OC remained stable at approximately 100 nm without notable changes. The mass-to-atom ratio of elemental S after OC cyclic reaction was found to be minimal, suggesting that the reduced OCs can be fully oxidized and regenerated after SO_2 release during the oxidation phase. XPS analysis further confirmed that, during the reduction process, there is an over-reduction of OCs by S, with a certain proportion of S elements present in the form of metal sulfides (FeS, Cu_2S). Consequently, SO_2 is released when the reduced OCs are oxidized by air in ARs, which occurs due to the oxidative regeneration of FeS and Cu_2S into Fe_2O_3 and CuO, respectively.

Author Contributions: Conceptualization, L.P. and M.Z.; methodology, L.P. and M.Z.; software, L.P.; validation, L.P. and M.Z.; formal analysis, L.P. and M.Z.; investigation, L.P.; resources, L.P. and M.Z.; data curation, L.P.; writing—original draft preparation, L.P.; writing—review and editing, L.P.; visualization, L.P.; supervision, M.Z.; project administration, M.Z.; funding acquisition, M.Z. All authors have read and agreed to the published version of the manuscript.

Funding: This research received no external funding.

Data Availability Statement: The original contributions presented in the study are included in the article, further inquiries can be directed to the corresponding author.

Conflicts of Interest: The authors declare no conflicts of interest.

References

1. Richter, H.J.; Knoche, K.F. Reversibility of combustion processes. In *Efficiency and Costing*; ACS Publications: Washington, DC, USA, 1983; pp. 71–85.
2. Gong, R.; Qin, C.; He, D.; Tan, L.; Ran, J. Oxygen Uncoupling of Cu-Based Oxygen Carrier with the Presence of Coal Ash in Chemical Looping Process. *Energy Fuels* **2018**, *32*, 7708–7717. [CrossRef]
3. Wang, B.; Yan, R.; Zhao, H.; Zheng, Y.; Liu, Z.; Zheng, C. Investigation of Chemical Looping Combustion of Coal with $CuFe_2O_4$ Oxygen Carrier. *Energy Fuels* **2011**, *25*, 240–246. [CrossRef]
4. Shen, L.; Wu, J.; Xiao, J. Experiments an Chemical Looping Combustion of Coal with a NiO Bosed Oxygen Carrier. *Combust Flame* **2009**, *156*, 721–728. [CrossRef]
5. Wang, B.; Yan, R.; Lee, D.H.; Zheng, Y.; Zhao, H.; Zheng, C. Characterization and Evaluation of Fe_2O_3/Al_2O_3 Oxygen Carrier Prepared by Solgel Combustion Synthesis. *J. Anal. Appl. Pyrolysis* **1996**, *91*, 105–113. [CrossRef]
6. Jiang, S.; Shen, L.; Wu, J.; Yan, J.; Song, T. The Investigations of Hematite-CuO Oxygen Carrier in Chemical Looping Combustion. *Chem. Eng. J.* **2017**, *317*, 132–142. [CrossRef]
7. Bhui, B.; Vairakannu, P. Prospects and issues of integration of Co-combustion of solid fuels (coal and biomass) in Chemical looping Technology. *J. Environ. Manag.* **2019**, *231*, 241–1256. [CrossRef] [PubMed]
8. Bukur, D.B.; Silvester, L.; Fischer, N.; Claeys, M.; Lemonidou, A.A. on the use of an in situ magnetometer to study redox and sintering proper-ties of NiO based oxygen carrier materials for chemical looping steam methane meforming. *Int. J. Hydrog. Energy* **2019**, *44*, 18093–18102. [CrossRef]
9. Lin, C. *Mechanism of Gas-Solid Reaction on the Surface of Iron-Based Oxygen Carriers with Chemical Chain Combustion Mutagenesis*; North China Electric Power University: Beijing, China, 2017; pp. 45–51.
10. de Diego, L.F.; Gayan, P.; Garcia-Labiano, F.; Celaya, J.; Abad, M.; Adanez, J. Impregnated CuO/Al_2O_3 oxygen carriers for chemical-looping combustion: Avoiding fluidized bed agglomeration. *Energy Fuels* **2005**, *19*, 1850–1856. [CrossRef]
11. Diego, L.D.; García-Labiano, F.; Gayán, P.; Abad, A.; Cabello, A.; Adánez, J.; Sprachmann, G. Performance of Cu- and Fe-based oxygen carriers in a 500 Wth CLC unit for sour gas combustion with high H_2S content. *Int. J. Greenh. Gas Control* **2014**, *28*, 168–179. [CrossRef]
12. Gayán, P.; Forero, C.R.; Diego, L.; Abad, A.; García-Labiano, F.; Adánez, J. Effect of gas composition in Chemical-Looping Combustion with copper-based oxygen carriers: Fate of light hydrocarbons. *Int. J. Greenh. Gas Control* **2010**, *4*, 13–22. [CrossRef]
13. Adánez-Rubio, I.; Abad, A.; Gayán, P.; García-Labiano, F.; de Diego, L.F.; Adánez, J. The fate of sulphur in the Cu-based chemical looping with oxygen uncoupling (CLOU) process. *Appl. Energy* **2014**, *113*, 1855–1862. [CrossRef]
14. Mendiara, T.; Izquierdo, M.T.; Abad, A.; De Diego, L.F.; García-Labiano, F.; Gayán, P.; Adánez, J. Release of pollutant components in CLC of lignite. *Int. J. Greenh. Gas Control* **2014**, *22*, 15–24. [CrossRef]
15. Garcia-Labiano, F.; de Diego, L.F.; Cabello, A.; Gayan, P.; Abad, A.; Adanez, J.; Sprachmann, G. Sulphuric acid production via Chemical Looping Combustion of elemental sulphur. *Appl. Energy* **2016**, *178*, 736–745. [CrossRef]

16. Suslick, K.S. *Kirk-Othmer Encyclopedia of Chemical Technology*; Wiley & Sons: New York, NY, USA, 1998; Volume 26, pp. 517–541.
17. Tian, X.; Wei, Y.J.; Zhao, H.B. Evaluation of a hierarchically-structured CuO@TiO_2-Al_2O_3 oxygen carrier for chemical looping with oxygen uncoupling. *Fuel* **2017**, *209*, 402–410. [CrossRef]
18. Wei, Z.; Liu, D.; Jing, J. Research progress on Fe-based oxygen carrier in chemical looping combustion. *Clean Coal Technol.* **2019**, *25*, 19–27.
19. Cheng, W.; Zhu, M.; Qin, W.; Hou, C. Chemical Looping Combustion Characteristics of Fe_2O_3(104) and CO Under Synergistic Action of ZrO_2/TiO_2 Carrier. Chem. *J. Chin. Univ.* **2018**, *39*, 506.
20. Zafar, Q.; Mattisson, T.; Gevert, B. Redox Investigation of Some Oxides of Transition-State Metals Ni, Cu, Fe, and Mn Supported on SiO_2 and $MgAl_2O_4$. *Energy Fuels* **2006**, *20*, 34–44. [CrossRef]
21. Zhao, S.Q.; Guo, S.J.; Zhu, C.; Gao, J.; Li, H.; Huang, H.; Liu, Y.; Kang, Z.H. Achieving electroreduction of CO_2 to CH_3OH with high selectivity using a pyrite-nickel sulfide nanocomposite. *Rsc Adv.* **2017**, *7*, 1376–1381. [CrossRef]
22. Jin, L.; Cai, L.; Chen, D.; Wang, W.; Shen, H.; Zhang, F. Efficient silicon solar cells applying cuprous sulfide as hole-selective contact. *J. Mater. Sci.* **2019**, *54*, 12650–12658. [CrossRef]